Soot formation and oxidation in oscillating methane–air diffusion flames at elevated pressure

Janbernd Hentschel, Rainer Suntz, and Henning Bockhorn

Comparisons with respect to the sooting tendency are made between stationary diffusion flames and diffusion flames with pulsations induced by oscillating fuel flow. Time-resolved measurements of the soot particle properties in the flames are obtained by combining Rayleigh-scattering, laser-induced incandescence, and extinction measurements into the RAYLIX method. Furthermore, flame luminosity at 590 nm and OH*-chemoluminescence signals at 310 nm are monitored to obtain data regarding the flame structure. Mean soot volume fractions of oscillating flames are significantly different from those of stationary flames with the same mean fuel flow rate; oscillations of the total amount of soot are phase shifted and asymmetric compared with fuel flow oscillations.

OCIS codes: 280.1740, 290.5870, 300.2140.

1. Introduction

As studies of laminar flames have considerably enhanced the understanding of the combustion processes, increased focus has been directed toward the understanding of more complex flame structures as they can be found in technically relevant geometries such as combustion engines and gas turbines. In these devices combustion occurs under nonstationary conditions.

To mimic nonstationary combustion the best results can be obtained by investigating repetitive, i.e., oscillating, flames, as they offer the possibility of applying phase-locked detection systems in order to obtain time-resolved data of nonstationary flames. This demands highly reproducible flames and challenges the experimental setup but, on the other hand, allows numerous or even mutually exclusive methods of detection to be applied consecutively.[1]

Experiments in the literature range from the natural pulsation frequency of flickering flames[2,3] to periodically forced flows. The latter can be differentiated by the frequency and amplitude and the method used to induce the oscillations. In most cases oscillations are forced with a membrane loudspeaker.[1,4–8] Two different frequency regimes were investigated in the literature, one close to the free-flickering frequency as defined in Refs. 2 and 3, the other with frequencies more than 1 order of magnitude higher than this frequency. For the amplitude at the burner exit it seems to be crucial to know whether it exceeds the average fuel flow rate, as a reversed flow back into the burner could cause the entrainment of the gas from the oxidizer flow. In such cases high amplitudes can cause premixing of the oxidizer and the fuel flow.[8,9]

With respect to pollutant formation in nonstationary flames, the main interest of investigations is directed toward soot properties and flame structures. As the effects of the different parameters in these flames interact and affect the flame properties in a complex way, no general tendencies can be fixed. Both soot reduction and soot enhancement can be found, depending on experimental setup, frequencies, and amplitudes.

The choice of methods to investigate the flame parameters is commonly based on optical techniques. This includes the recording of properties of radiation emitted by the flame, which are, e.g., soot luminosity and OH chemoluminescence (OH*). Cw light source techniques, such as the schlieren technique and extinction measurements, are used as well as pulsed-laser-based methods like laser-induced incandescence (LII), Rayleigh-scattering, and laser-induced fluorescence experiments. They have in common that they can, directly or indirectly, derive spatially resolved data and, most important, have acquisition times short

The authors are with the Institut für Technische Chemie und Polymerchemie, Universität Karlsruhe (TH), Kaiserstraße 12, 76128 Karlsruhe, Germany. J. Hentschel's e-mail address is hentschel@ict.uni-karlsruhe.de.

Received 2 February 2005; revised manuscript received 11 May 2005; accepted 13 May 2005.

0003-6935/05/316673-09$15.00/0

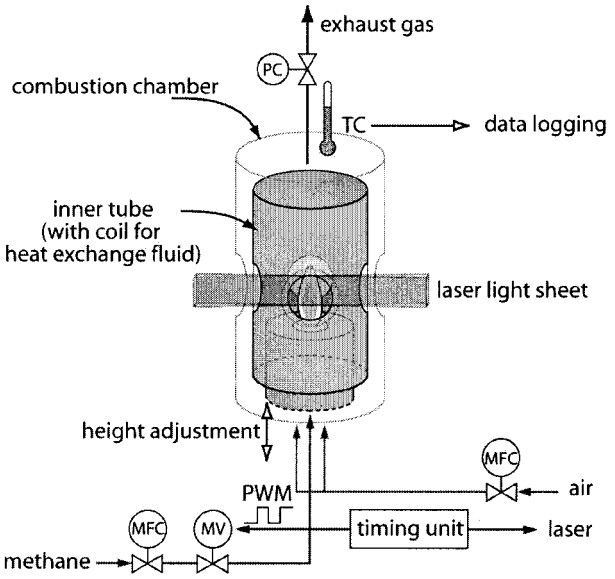

Fig. 1. Setup of the burner inside the pressure chamber (TC, thermocouple; MFC, mass flow controller; PC, pressure controller; MV, magnetic valve; PWM, pulse-width modulation).

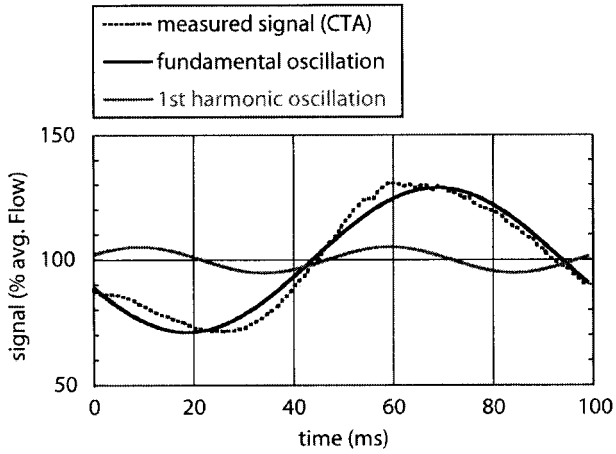

Fig. 2. Results from the CTA at 2 mm above the center of the burner. The axial velocity component is given as percent of the average velocity.

enough in comparison to the variation of the flow field to yield time-resolved data.

2. Experiment

This paper focuses on the investigation of oscillating flames with weak and low-frequency forcing. They are investigated by means of the soot luminosity, the OH* emission, and the RAYLIX technique, the latter being a combination of Rayleigh-scattering, LII, and extinction.[10,11] The determination of the fuel flow rate variations at the burner exit is done by hot wire anemometry. Experiments are carried out in sooting laminar methane–air diffusion flames at an elevated pressure of 2.5 bars (1875 torr).

A. Burner and Housing

The flames are stabilized inside a pressure chamber, which consists of three parts. In the lower part of the chamber is the burner adjustment and gas supply. The middle part is equipped with four windows, which are perpendicular to one another, and a tube containing the burner head. On top a unit for exhaust gas cooling and leveling is located. The pressure chamber itself is kept at a constant temperature of 80 °C to prevent condensation of water from the exhaust gas. The windows are antireflection coated to avoid secondary reflections inside the burner chamber.

The tube surrounding the burner is independently temperature controlled by a coiled tube for heat exchange. The tube has four circular cuts in line with the windows of the pressure chamber to allow optical access and fits tightly around the burner. This setup is shown in Fig. 1, where a schematic view of the inner tube, the light sheet for the RAYLIX measurement, the burner, and the gas flow chart can be seen.

The burner consists of two concentric sintered metal plates, the inner one having an open diameter of 10 mm, the outer plate with an inner diameter of 22 mm and an outer diameter of 50 mm. The cold gas flows are 0.2 1_N/min and 12 1_N/min for methane and air, respectively.

In order to induce the oscillations of the flame, the fuel gas flow is periodically modulated. The methane flow is pulse width modulated by a magnetic valve outside the pressure chamber. The flow rates of the cold methane flow have been determined by constant temperature anemometry (CTA) measurements 2 mm above the center of the burner, where the axial velocity component of the flow has been recorded. Because of the large volume of the pressure chamber, the measurements can be regarded as isobaric.

Figure 2 shows that the pulse-width modulation of the gas feed further upstream results in a flow rate that can be fitted as the sinusoidal oscillation and, to a minor extent, its few first harmonics. In the plot in Fig. 2 the recorded signal of the CTA, the fundamental oscillation, and the first-harmonic oscillation are shown. The latter two have been calculated from a Fourier-transform analysis of the CTA signal. Higher harmonics were not found; this is a consequence of the low-pass characteristics of the valve mechanics, the volumes in the tubing, and flow resistances rather than of the limited temporal resolution of the CTA. Amplitudes and phases of the resulting flow can be varied by changing the pulse width and the average flow. This arrangement avoids resonant behavior and nodal points that can be found in speaker-driven systems. The frequency of the oscillations investigated in this work is 10 Hz. The fuel gas flow rate is modulated with an amplitude of 30% of the average gas flow. The excitation frequency is chosen to be close to the frequency of self-induced flickering in these flames. This frequency is given by $f = 1.5 \times D^{-1/2}$, D being the dimension of the fuel nozzle in meters.[2,3] This leads, in the present case, to a free-flickering frequency of 15 Hz. Some corrections might possibly be necessary to account for the higher buoyancy of the flame caused by the higher pressure but

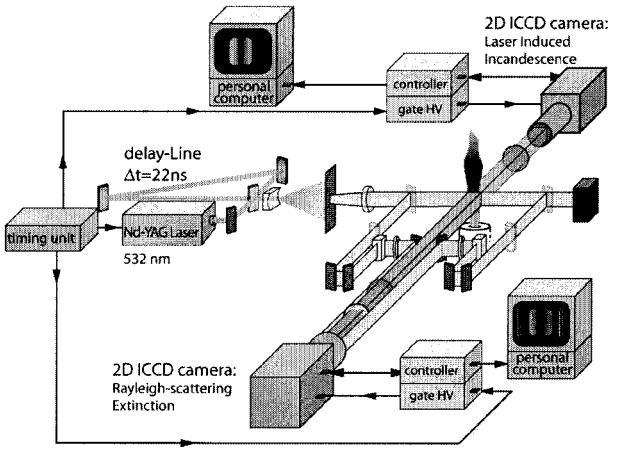

Fig. 3. Setup of the RAYLIX techniques. A laser beam from a frequency-doubled Nd:YAG laser is split into two partial beams. One of them is delayed by 20 ns with respect to the other. Both beams pass a telescope and form a light sheet with a smooth focus line inside the flame. The first beam induces the Rayleigh scattering and is used for the evaluation of the extinction. Both signals are recorded with one intensified CCD camera. The LII signal is detected with a second camera after the induction by the delayed beam.

do not lie within the scope of this paper. Observations of freely flickering flames in this setup suggest a frequency of self-induced flickering in the 10–20 Hz frequency range.

The excitation amplitude and frequency of the oscillating flames used in this work are in accordance with the above-mentioned classification in the low-frequency and low-excitation-level regime.

B. RAYLIX

The properties of primary soot particles, i.e. median radii, number densities, and soot volume fractions, are measured with the RAYLIX technique. It was described in detail previously[10,11] and is based on the nearly simultaneous detection of Rayleigh scattering, LII, and extinction by using a single laser pulse. The nearly simultaneous ($\Delta t = 20$ ns) acquisition of signals outruns the flow speed and chemistry in the nonstationary flames under investigation. The setup of this method is shown in Fig. 3 and is described in the following. The Rayleigh and LII signals are induced by a frequency-doubled Q-switched Nd:YAG laser (532 nm) with a pulse duration of 11 ns FWHM. The laser beam is split into two beams to sequentially induce the Rayleigh-scattering signal and, with the stronger part of the laser beam being delayed by 20 ns after passing the delay line, the LII signal. The extinction measurements are performed by detecting the intensity of the first beam before and after it passes the burner chamber.

Both laser beams pass a Galileo telescope consisting of a cylindrical concave lens and a spherical convex lens and an aperture, yielding a laser sheet with uniform intensity over the height and a smooth focus line in the flame. The sheet has an almost constant thickness of 60 μm in the region of the flame, assuming a Gaussian beam profile.

The Rayleigh-scattered signal is detected by an intensified CCD (ICCD) camera perpendicular to the laser sheet. An appropriately chosen intensity of the laser beam on both sides of the pressure chamber is recorded simultaneously on the camera chip. The latter signals are used for the estimation of the extinction. A bandpass filter at 532 nm suppresses the background signal of the luminosity of the soot particles and transmits the Rayleigh-scattered light. A 15 ns gate width of the image intensifier at the time of the laser pulse enhances the signal-to-noise ratio.

The incandescence signal is induced by the more intense, delayed laser beam. The LII is detected at the wavelength between 400 and 430 nm by a second ICCD camera on the opposite side of the flame with respect to the Rayleigh camera. The shutter of this camera is opened 10 ns after the laser pulse passed the flame and the camera chip is exposed for 100 ns. The cameras are adjusted carefully so that the images align with each other; the area projected onto each pixel is 80 μm × 80 μm. The high reproducibility and stability of both the pulsating and the stationary flame allow the mean value of 50 single shots to be used to enhance the signal-to-noise ratio. The images of the total flame height (6 cm) are put together from several overlapping stripes, each of them being 1.2 cm high.

Images of the pulsating flame are taken at selected phase angles of the oscillating fuel flow by trigger signals appropriately sent to the laser–camera system. The phase-locked acquisition of the data gives a time-resolved evolution of the flame characteristics, which can be related to the fuel flow as it has been measured by CTA.

C. Soot Luminosity and OH* Emission

Soot luminosity and the emission of electronically excited hydroxyl radicals (OH*), i.e., the chemoluminescence, are consecutively detected by a single ICCD camera. A set of four bandpass mirrors and one additional low-wavelength pass filter results in a highly efficient filter[12] for the detection of the OH* emission with a center wavelength at 310 nm (FWHM 10 nm, peak transmission 60%). The set of four mirrors has a second bandpass region (center at 590 nm, FWHM 50 nm), which, after the low wavelength pass filter is removed, can be used for the detection of the soot luminosity. The OH* radiation differs more than 3 orders of magnitude from the soot luminosity, and its effect on the determination of the luminosity can be neglected. The luminosity of the soot particles is used as a qualitative indicator for hot soot particles, while the emission of the excited hydroxyl radical, after tomographic reconstruction, can be used to visualize the structure of the reaction zones in the flame.[13]

The image acquisition is similar to that for the RAYLIX images. The gated image intensifier of the ICCD camera is phase locked to the oscillation cycle to evaluate the time-resolved evolution of the flame, and the images are assembled from 1.2 cm high, over-

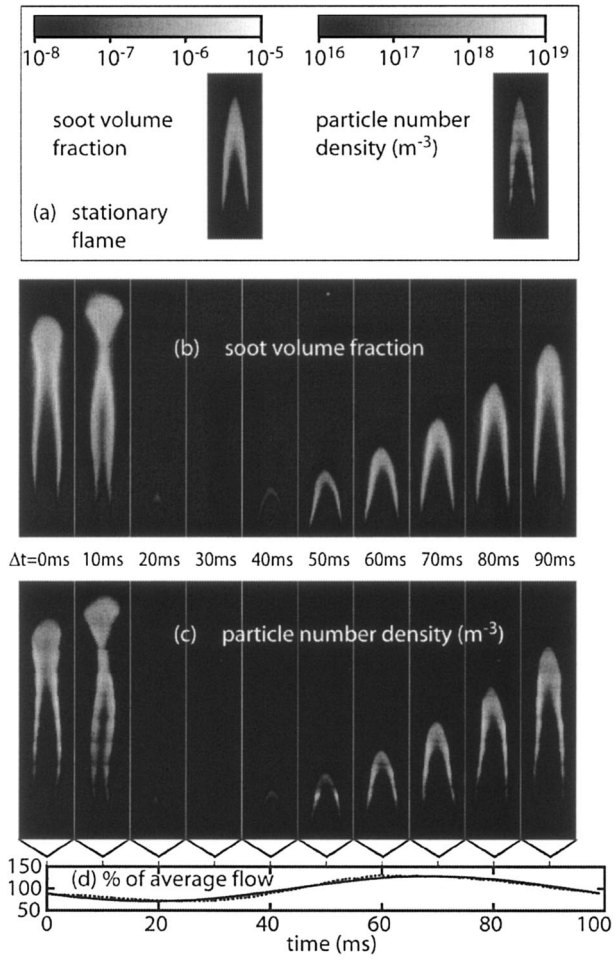

Fig. 4. Results from the RAYLIX measurements. (a) Soot volume fraction and particle number densities in the stationary flame. (b) Soot volume fractions in the oscillating flame. The time interval between the images is 10 ms. (c) Corresponding particle number densities. (d) Results from the CTA as seen in Fig. 2.

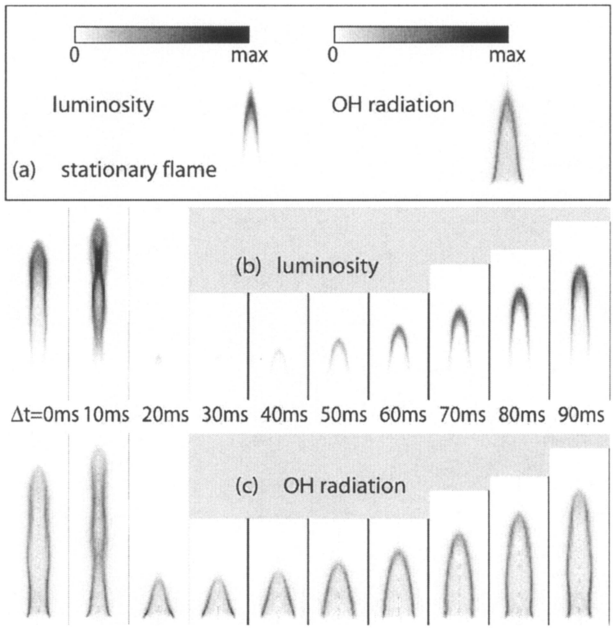

Fig. 5. (a) Luminosity and OH* emission in the stationary flame. (b) Luminosity in the oscillating flame. The time interval between the images is 10 ms. (c) Corresponding images of the OH* radiation.

lapping sections, averaged from 50 single images. Because the camera is a different distance from the burner, the area projected onto each pixel is increased to 100 μm × 100 μm. An onion-peeling method is used according to Ref. 14 to deconvolve the projection view of the camera into the two-dimensional cross sections of the flames. The onion-peeling method is used because of its minimal smoothing of steep edges. Though the assumption of cylindrical symmetry is almost fulfilled for the experimental results, the average of the left- and the right-hand sides is taken for reconstruction of the profiles. Deviations caused by a limited depth of focus and in-flame extinction of the signals are neglected, and no absolute calibration is performed. Therefore these results are analyzed on a qualitative basis.

3. Results and Discussion

Figure 4 shows the soot volume fractions and the particle number densities as obtained from the RAYLIX measurements. At the top the results of the corresponding steady flames are shown; the two next rows show the soot volume fraction [Fig. 4(b)] and the particle number density [Fig. 4(c)] in the forced flame. The stationary and the oscillating flames have the same mean fuel flow rates. The temporal evolution of the oscillating flame is recorded with a time intervall of 10 ms (equivalent to a phase angle of 36°) by phase-locked acquisition, the first image starting at $\Delta t_0 = 0$ ms. In the last row the data for the fuel flow rate from the CTA measurements is plotted.

Figure 5 shows the corresponding images of the flame luminosity at 590 nm and the OH* emission profiles derived from the onion-peeling deconvolution. As they are not calibrated, no absolute scale is given. In these images the gray-scale gradient is linear to the signal intensity.

Because of the fast collapse of the flame between $\Delta t = 10$ and $\Delta t = 20$ ms, the corresponding images of the flame at the time of $\Delta t = 15$ ms are shown in Fig. 6. They would fit between the second and third images in the temporal sequences in Figs. 5. In this time step the upper part of the flame detaches from the base of the flame, and it seems that the soot is being oxidized from the circumference.

The comparison of the LII signals from the RAYLIX measurements (Fig. 4) and the luminosity of the flames (Fig. 5) shows good agreement with respect to the presence and absence of soot. The presence of the LII signal in places where no luminosity is observed would indicate the presence of cold soot particles outside the regions in which combustion takes place. Its absence indicates that no considerable amount of soot is found outside the flames and that no remarkable emission of particulate matter takes place. This is in accordance with the fact that no notable deposition of

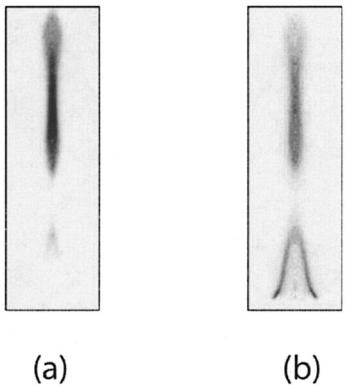

Fig. 6. Images of the (a) luminosity and (b) OH* emission. The images are taken at a delay of $\Delta t = 15$ ms; they fit between the second and third frames in Figs. 5(b) and 5(c).

soot is found inside the pressure chamber and the exhaust tubing. On the other hand, it shows that the onion-peeling deconvolution works quite well for these flames.

The first impressions gained from the images of the soot volume fraction are that the oscillating flame almost completely lifts off the burner and that the combustion is nearly extinguished at the flame base between $\Delta t = 15$ and $\Delta t = 30$ ms. In contrast to the soot volume fraction, the OH* emission recordings show that the conical reaction zone at the flame base remains intact while the upper part of the flame detaches.

For a quantitative description of the effects found, two methods have been used. First, the value of the maximum soot volume fraction of the profiles at each height above the burner has been plotted as a function of the hight above the burner for several phases of the flame during the oscillation and the stationary flame. This plot is shown in Fig. 7, the height being assigned to the upright axis. It can be seen that the maximum soot volume fraction in the oscillating flames is about half an order of magnitude higher than in the stationary flame at several times during the cycle. Especially notable is the data from the flame at $\Delta t = 70$ ms. Though it is of a height similar to that of the stationary flame, its peak soot volume fraction is three times higher. One can conclude that even moderately transient initial conditions can influence the soot formation and oxidation significantly.

Further quantification is given by the data as seen in Figs. 8–10. Here the total amount of soot (Fig. 8) and the total particle number (Fig. 9) inside the laser sheet (i.e., the sum of all pixels in the image multiplied by the detection volume) and the total emission of the OH* (Fig. 10) of every phase of the oscillating flame is normalized by the corresponding value from the stationary flame and is plotted as a function of time. Additionally, in case of the soot volume fraction, the fuel flow rate is given in a second plot.

The fuel flow rate oscillates quite symmetrically, while the total amount of soot shows a distinct asymmetric behavior and a phase lag of about 35 ms in its

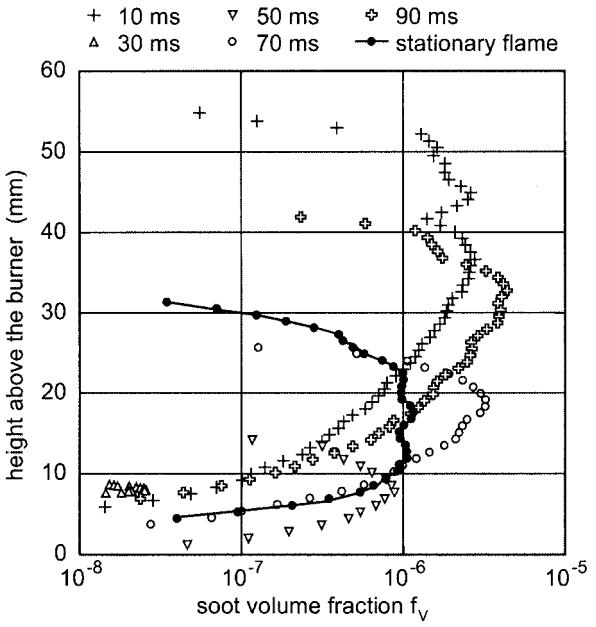

Fig. 7. Maximum value of the soot volume fraction for each height above the burner plotted against its height (on the upright axis).

maximum values. The amount of soot in the oscillating flame is up to seven times higher than the corresponding value in the stationary flame. Even though almost no soot is present in the flame between $\Delta t_0 = 20$ ms and $\Delta t_0 = 50$ ms of the oscillation cycle, the time-averaged concentration during one cycle, plot-

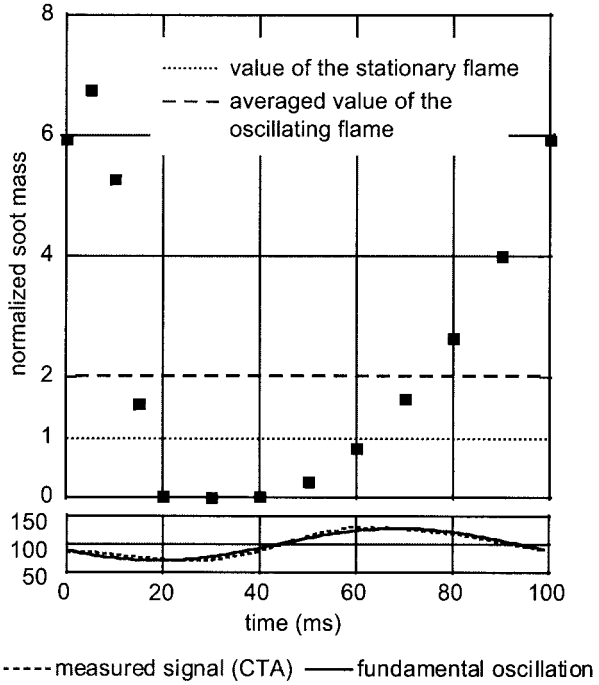

Fig. 8. Temporal evolution of the soot mass in the cross section given by the light sheet during one period. The data are normalized to the value of the stationary flame. The dashed line indicates the time-averaged value of one period. For comparison the data of the CTA as in Fig. 2 are given.

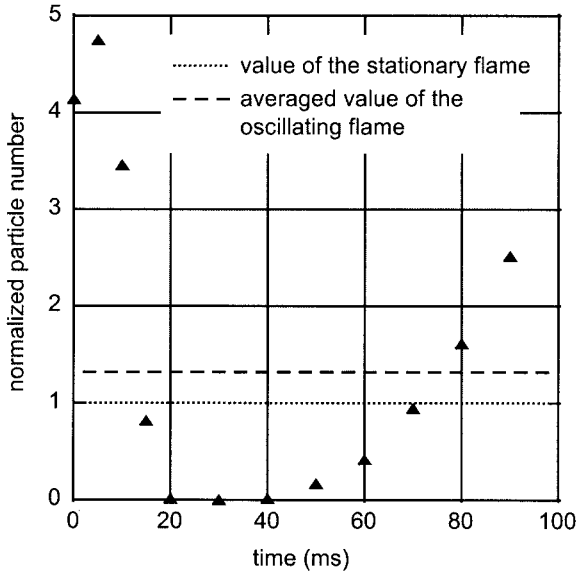

Fig. 9. Temporal evolution of the particle numbers in the cross section given by the light sheet during one period. The data are normalized to the value of the stationary flame. The dashed line indicates the time-averaged value of one period.

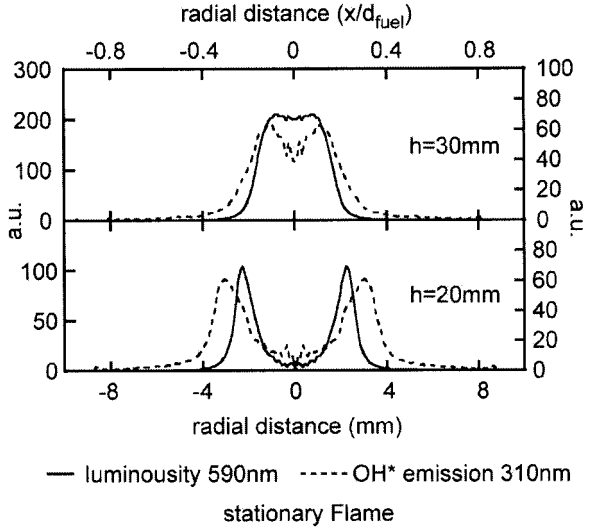

Fig. 11. Profiles of luminosity at 590 nm and OH* emission in arbitrary units at two different heights above the burner (as given in the figure) for the stationary flame.

ted as the dashed line, is more than two times higher than in the stationary flame. This applies, to a minor extent, in the same way to the particle numbers as displayed in Fig. 9.

Three main points stand out. First, there is a time lag of about 35 ms between the fuel flow rate and the soot formation and oxidation. Second, the fuel flow rate has a nearly sinusoidal shape. The increase of the soot volume and the particle number are highly asymmetric; a steep decline during the collapse of the flame is followed by a slow exponential increase.

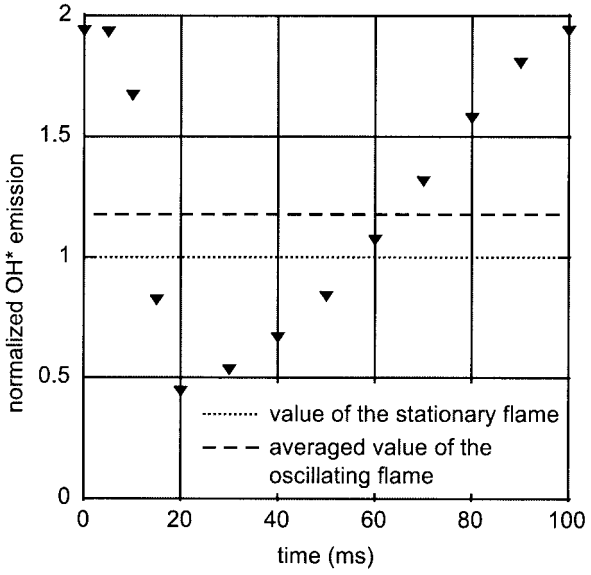

Fig. 10. Temporal evolution of the total OH* emission in the flame during one period. The data are normalized to the value of the stationary flame. The dashed line indicates the time-averaged value of one period.

Third, the amplitude of the fuel flow rate is 30% of the mean gas flow; i.e., the maximum fuel flow rate is less than two times the minimum value. The maximum values of the soot mass and particle number during the oscillation are several times higher than in the stationary flame, and the minima are close to zero.

To a minor extent, a similar behavior can be found in the plot of the overall OH* emission of the flame. The time lag is the same; however, the increase after the collapse of the flame is linear rather than exponential, and the amplitude relative to the mean value is lower than those of the soot parameters but still larger than that of the fuel flow rate. The differences are mainly due to the fact that the peak values of the OH* emission for each frame do not change as much as those of the soot concentration. The soot mass in the flames increases by an a simultaneous enlargement of the soot zone and increase in the soot concentration in these zones. The OH* emission instead increases almost exclusively by the enlargement of the reaction zone but not by higher peak values. Therefore the relative increase of the OH* emission is smaller, and the peak value of the total OH* emission during the cycle is enhanced only by a factor of 1.9 compared with the stationary flame.

This is an indication of different behaviors of the soot and the gas phase species. To allow us to further investigate this phenomenon several profiles of the OH* emission and the luminosity have been plotted in Figs. 11 to 13. Some representative states of the flames have been chosen, two in the buildup phase $\Delta t = 50$ ms and $\Delta t = 0$ ms of the flame, two in the collapsing phase ($\Delta t = 10$ ms and $\Delta t = 1.5$ ms), and the stationary flame as reference. Except for the flame at $\Delta t = 50$ ms, for each flame two profiles have been chosen, one in the top region of the flame where the soot is oxidized and one at the flame base where two distinct reaction zones are present. For the flame

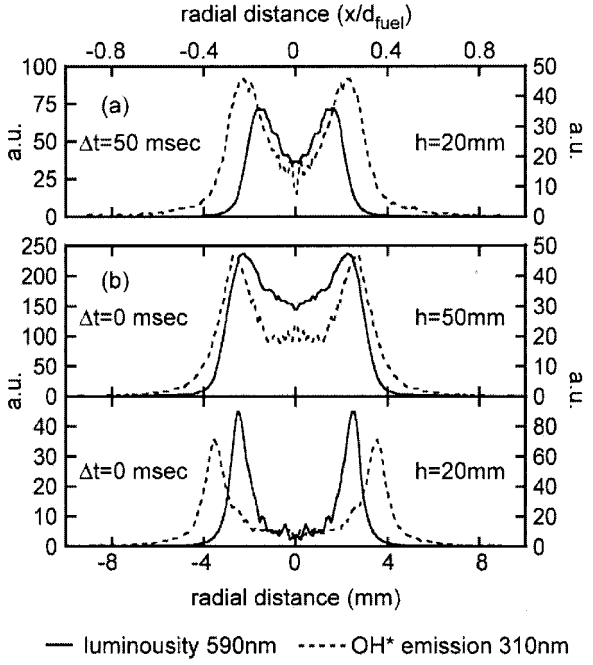

Fig. 12. Profiles of luminosity at 590 nm and OH* emission in arbitrary units at two different heights above the burner (as given in the figure) for the oscillating flame during the build up phase at (a) $\Delta t = 50$ ms and (b) $\Delta t = 0$ ms.

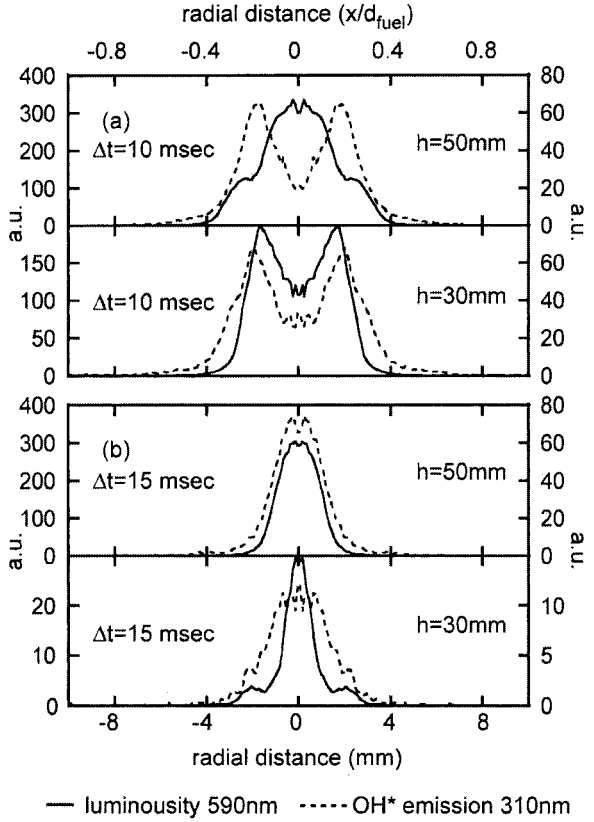

Fig. 13. Profiles of luminosity at 590 nm and OH* emission in arbitrary units at two different heights above the burner (as given in the figure) for the oscillating flame during the collapsing phase at (a) $\Delta t = 10$ ms and (b) $\Delta t = 15$ ms.

at 50 ms only the latter has been chosen because of the limited height of the flame. All plots are in arbitrary units, as only qualitative analysis has been performed.

It has to be noted that the OH* radicals are formed through a different reaction path than the ground-state OH radicals; OH* is formed by the oxidation of CH radicals,[15] which can be taken, therefore, as reference for the approximate location of the OH* radical. This avoids the calculation of the profiles of OH*, which is not performed in the corresponding flamelet calculations. Figure 14 shows as an example the stationary methane–air flamelet at 2.5 bars (1875 torr) and a scalar dissipation rate of 1 s^{-1}. The OH concentration, CH concentration (as reference for OH*), and soot volume fraction are plotted against the mixture fraction. A mixture fraction of 0 represents the pure oxidizer flow outside the flame, and 1 indicates pure fuel flow at the core of the flame base. It can be seen that the CH separates the area of soot from the oxidizing regimes where OH radicals can be found.

At the base of the steady flame (Fig. 11) the OH* layer is found to enclose the sooting layers of the flame. At the maximum OH* emission the soot luminosity almost vanishes. If soot particles were present in this hot reaction zone, then they should be luminous and therefore appear in this plot. These findings comply with results expected from flamelet calculations as plotted in Fig. 14.

In the top of the steady flame (Fig. 11) both layers have moved toward the center; the soot layers are fused together, while the OH* emission still has two peaks and lies slightly further away from the center of the flame than the soot. At the place of the maximum OH* radiation the luminosity still shows a good part of the peak luminosity in that profile; i.e., the soot layer begins to overlap with the OH* layer.

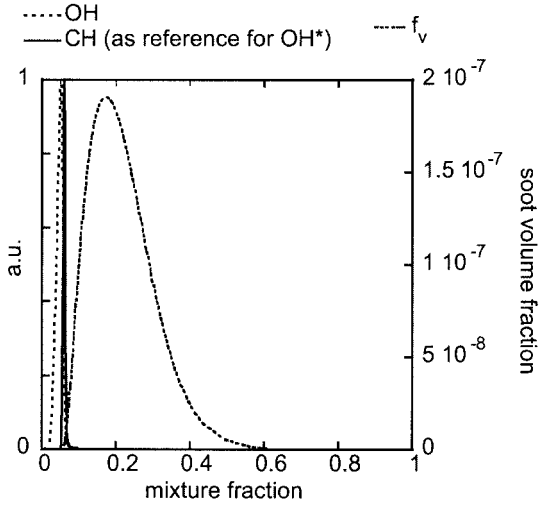

Fig. 14. OH and CH concentration (arbitrary units) and soot volume fraction as a function of mixture fraction; calculated as a stationary methane–air flamelet at 2.5 bars (1875 torr) scalar dissipation rate 1 s^{-1} with the SOFOKLES code.[16]

The same is valid for the two plots in Fig. 12, which are profiles taken at the beginning [Fig. 12(a)] and the end [Fig. 12(b)] of the buildup phase. In the flame base in Fig. 12(b) the two distinct peaks of the soot luminosity are found to be accompanied by the two OH* emission peaks further outward. Again, with increased height above the burner the soot layers are fused into each other, directly enclosed by the OH* layer. The plot in Fig. 12(a) can be seen as lying between those two profiles at a medium height.

The plots change remarkably when profiles from the collapsing flames are plotted. The set of plots in Fig. 13(a) are at $\Delta t = 10$ ms [i.e., 10 ms after the images in Fig. 12(b)], followed by those in Fig. 13(b) after an interval of 5 ms at an absolute delay of $\Delta t = 15$ ms. At the beginning of the collapse of the flame the profiles at the flame base are typical for those found in the soot oxidation zone in the top of the other flames; the luminosity and OH* emission peaks are less distinct from each other. This appearance changes further at the top of the flame. The soot luminosity has blended into a single peak with shoulders in the place of the maximum of the OH* emission. The outer edges of the two profiles coincide.

Five milliseconds later plots from both the flame top and the base in Fig. 13(b) show only a single peak of luminosity, and even the OH emission peaks have blended into one peak with the maximum at the flame center. In the profiles at the base of the flame a shoulder can be found, approximately at the place where the maximum of the OH emission had been 5 ms earlier. Both profiles of the soot luminosity have narrowed to a fraction of their predecessors 5 ms earlier.

This does indicate that the combustion process in the collapsing flame is no longer to be described as that of a complete diffusion flame but as that of the soot oxidation zone found in the tip of stationary diffusion flames. During this process the soot in the detached part of the flame is burned from the outside toward the center of the flame.

4. Conclusion

Oscillating flames have been compared with a stationary flame with the same mean flow rate. Measurements of soot volume fraction, particle number densities, OH* emission, and soot luminosity have been performed. Additionally, the velocities of the cold fuel gas flow were acquired by CTA measurements.

The oscillating flame has a peak soot volume fraction three times higher than the stationary flame at a time when it has the same height as the stationary flame. Therefore the history of the flame evolution determines the combustion process rather than the actual state.

Comparing the fuel gas flow, the soot mass, the particle numbers, and the OH* emissions, three main differences were observed.

First, the flame follows the oscillation of the fuel gas flow at the burner exit with a time lag of approximately 35 ms between the maxima of the oscillation.

Second, the fuel gas oscillates symmetrically, but the flame shows an asymmetric oscillation.

Third, the soot mass and particle numbers vary by more than 2 orders of magnitude, while the oscillation of the fuel gas flow that initiates these changes has amplitudes of 30% of the average flow rate.

The comparison of profiles of the luminosity and the OH* radiation divides the evolution of the oscillating flame into two phases, the phase of the flames' building up and of their collapse. In the first they show a behavior comparable with that of the steady flame, while in the latter they have to be compared with the soot oxidation zones of the stationary flame. The soot in the detaching part of the flame is oxidized from the outside until it vanishes.

This work was performed within the scope of Sonderforschungsbereich 606 on nonstationary combustion, and we gratefully acknowledge the financial support of the Deutsche Forschungsgemeinschaft.

References

1. U. Vandsburger, J. M. Seitzman, and R. K. Hanson, "Visualization methods for the study of unsteady nonpremixed jet flame structure," Combust. Sci. Technol. **59,** 455–461 (1988).
2. A. Hamins, J. C. Yang, T. Kashiwagi, "An experimental investigation of the pulastion frequency of flames," in *Proceedings of 24th Symposium (International) on Combustion 1992* (Combustion Institute, 1993), pp. 1695–1702.
3. B. M. Cetegen and T. A. Ahmed, "Experiments on the periodic instability of buoyant plumes and pool fires," Combust. Flame **93,** 157–184 (1993).
4. C. R. Shaddix, J. E. Harrington, K. C. Smyth, "Qunatitative measurements of enhanced soot production in a flickering methane/air diffusion flame," Combust. Flame **99,** 723–732 (1994).
5. O. A. Ezekoye, K. M. Martin, and F. Bisetti, "Pulsed flow modulation of soot production in a laminar jet-diffusion flame," in *Proceedings of 30th Symposium (International) on Combustion 2004* (Combustion Institute, 2005), pp. 1485–1492.
6. B. A. Strayer, D. Dunn-Rankin, and F. Jabbari, "A comparison between frequency- and amplitude-modulated adaptive control of a non-premixed flame," in *Proceedings of 27th Symposium (International) on Combustion 1998* (Combustion Institute, 1999), pp. 1247–1254.
7. T. K. Kim, J. Park, and H. D. Shin "Mixing mechanism near the nozzle exit in a tone excited nonpremixed jet flame," Combust. Sci. Technol. **89,** 83–100 (1993).
8. M. Saito, M. Sato, and A. Nishimura, "Soot suppression by acoustic oscillated combustion," Fuel **77,** 973–978 (1998).
9. G. Papadopoulos, R. A. Bryant, and W. M. Pitts, "Flow characterization of flickering methane/air diffusion flames using particle image velocimetry," Exp. Fluids **33,** 472–481 (2002).
10. H. Geitlinger, T. Streibel, R. Suntz, and H. Bockhorn, "Two-dimensional imaging of soot volume fractions, particle number densities, and particle radii in laminar and turbulent diffusion flames," *in Proceedings of 27th Symposium (International) on Combustion 1998* (Combustion Institute, Pittsburgh, 1999), pp. 1613–1621.
11. H. Bockhorn, H. Geitlinger, B. Jungfleisch, T. Lehre, A. Schön, T. Streibel, and R. Suntz, "Progress in characterization of soot formation by optical methods," Phys. Chem. Chem. Phys. **4,** 3780–3793 (2002).
12. A. Arnold, B. Lange, T. Bouché, T. Heitzmann, G. Schiff, W. Ketterle, P. Monkhouse, and J. Wolfrum: "Absolute temperature fields in flames by 2D-LIF of OH using excimer lasers and CARS spectroscopy," Ber. Bunsenges. Phys. Chem. **96,** 1388–1393 (1992).

13. R. K. Hanson, "Combustion diagnostics planar imaging techniques," in *Proceedings of 21st Symposium (International) on Combustion 1986* (Combustion Institute, 1988), pp. 1677–1691.
14. C. J. Dasch, "One-dimensional tomography: a comparison of Abel, onion-peeling, and filtered backprojection methods," Appl. Opt. **31,** 1146–1152 (1992).
15. D. S. Dandy, S. R. Vosen, "Numerical and experimental studies of hydroxyl radical chemoluminescence in methane air flames," Combust. Sci. Technol. **82,** 131–150 (1992).
16. J. Appel, H. Bockhorn, and M. Frenklach, "Kinetic modeling of soot formation with detailed chemistry and physics: laminar premixed flames of C2 hydrocarbons," Combust. Flame **121,** 122–136 (2000).